FDC Particle Identification via dE/dX – v2.0

Daniel S. Carman
Department of Physics, Ohio University
April 19, 2005

1 Introduction

This document explores some issues related to employing the GlueX Forward Drift Chambers (FDCs) as a system for charged particle identification. The primary method considered here is to measure the specific ionization (dE/dX) to separate charged hadrons (pions, kaons, and protons) by utilizing the fact that different particles can be identified in a drift chamber because of the special relationship between dE/dX and $\beta\gamma$ (the relativistic generalization of velocity) or between dE/dX and momentum P. The ionization energy loss of charged particles can be measured in the FDC system by pulse-height sampling.

The issue of employing the FDC system as a particle identification device (or even to provide supplementary or complementary particle identification information) has arisen due to the present difficulties with the planning for the downstream Cerenkov detector in the GlueX detector system.

This document is meant to provide some insight into how well the current FDC design can provide useful $\pi/K/p$ separation, or more specifically, over what range can the current FDC design reasonably separate the different particle species. It can be expected to be updated as new work is completed and new ideas are considered.

2 Current FDC Design

The Forward Drift Chamber system (FDC) is used to track charged particles coming from the GlueX target with polar angles up to 30°. Due to the spiraling trajectories of the charged particles and the high multiplicity of charged tracks passing through the FDC, it is crucial for this system to be able to provide a sufficient number of measurements with appropriate redundancy to enable linking of the hits from the different tracks with high accuracy, while providing good spatial resolution with reasonable direction information. The goal is to design a system with position resolution accuracy of 150 μm for each space point.

In the current detector design, the FDCs include four separate but identical disk-shaped planar drift chambers (MWDC's) as shown in Fig. 1. Each 1.2 m diameter package will include six layers of alternating anode and field-shaping wires sandwiched between planes of cathode strips. The total thickness of each package is estimated to be roughly 0.15 gm/cm^2. The thickness of each tracking layer (24 in total from 4 packages with 6 layers per package) is 2.0 cm.

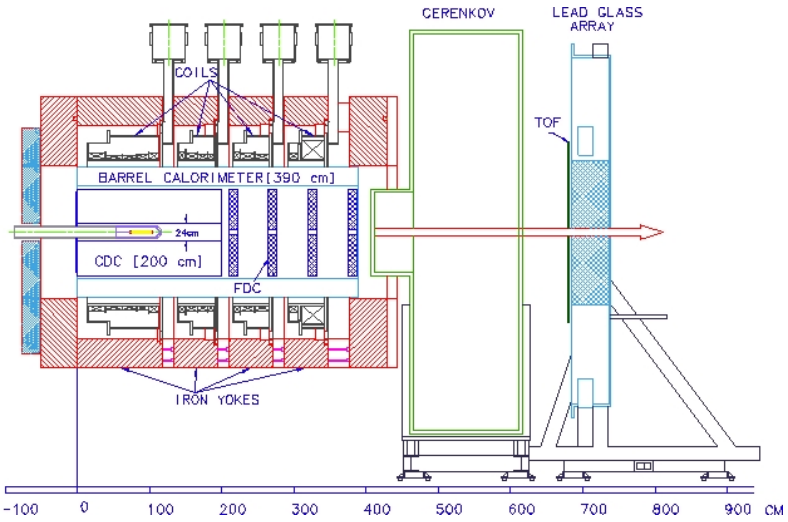

Figure 1: Schematic side view of the GlueX detector system showing the nominal FDC setup as currently planned.

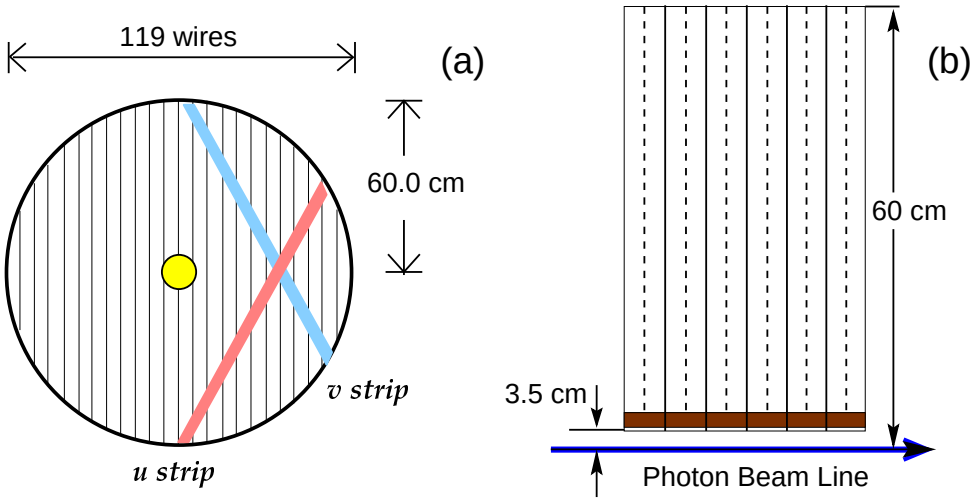

Figure 2: A front (a) and side (b) sketch of an FDC package. In (a) the wires are schematically indicated as the vertical lines. In (b) a side view of the upper half of a six-chamber package is shown. The wire planes are shown as the dashed lines, while the cathode planes are shown as the solid lines.

3 Stopping Power Theory

Moderately relativistic charged hadrons lose energy in matter primarily through multiple collisions with the atomic electrons of the medium (i.e. via ionization). The mean rate of energy loss (also called the stopping power) is given by the Bethe-Bloch formula,

$$-\frac{dE}{dX} = 2\pi N_A r_e^2 m_e c^2 \rho \frac{Z}{A}\frac{z^2}{\beta^2}\left[\ln\left(\frac{2m_e\gamma^2\beta^2 W_{max}}{I^2}\right) - 2\beta^2\right], \quad (1)$$

with $2\pi N_A r_e^2 m_e c^2 = 0.1535$ MeV cm^2/gm. The terms in this expression are defined in Table 1.

r_e : classical electron radius (2.817×10^{-13} cm)	ρ : density of medium
m_e : electron mass	ze : charge of incident particle
N_A : Avogadro's number	β : v/c of incident particle
I : Mean excitation potential	γ : $1/\sqrt{1-\beta^2}$
Z : Atomic number of medium	δ : density correction
A : Atomic weight of medium	C : shell correction
	W_{max} : max. energy transfer

Table 1: Terms in the Bethe-Bloch formula for stopping power.

The maximum energy transfer W_{max} from the incident hadron to an electron that can be provided in a head-on collision. For an incident particle of mass M, this can be computed as:

$$W_{max} = \frac{2m_e c^2\eta}{1 + 2s\sqrt{1+\eta^2} + s^2}, \quad (2)$$

where $s = m_e/M$ and $\eta = \beta\gamma$.

In practice two corrections are made to this expression to account for density effects (δ) and shell corrections (C). The notion of density effects, which are important as the energy of the incident charged particle increases, arises from the fact that the electric field of a charged particle tends to polarize the atoms along its path. Due to this effect, electrons far from the path of the particle are shielded from the full electric field intensity. The notion of shell effects, which are most important at low energies, is needed to account for effects that arise when the velocity of the incident particle is comparable to the electron's orbital velocity. In this case the atomic electrons cannot be assumed as stationary.

The modified form of the Bethe-Bloch equation including the density and shell correction terms then becomes [1]:

$$-\frac{dE}{dX} = 2\pi N_A r_e^2 m_e c^2 \rho \frac{Z}{A}\frac{z^2}{\beta^2}\left[\ln\left(\frac{2m_e\gamma^2\beta^2 W_{max}}{I^2}\right) - 2\beta^2 - \delta - 2\frac{C}{Z}\right]. \quad (3)$$

Fig. 3 shows a computation of the stopping power, actually $(1/\rho)dE/dX$, vs. momentum for pions, kaons, and protons in an Argon/CO_2 (90-10) gas mixture. The filled bands represent the measurement resolution (defined in Section 4). At non-relativistic energies,

dE/dX is dominated by the leading $1/\beta^2$ factor and decreases with increasing velocity until about $v = 0.96c$, when a minimum is reached. Here the particles are referred to as minimum ionizing. As the momentum increases beyond this point, dE/dX begins to increase (called the relativistic rise) due to the logarithmic term.

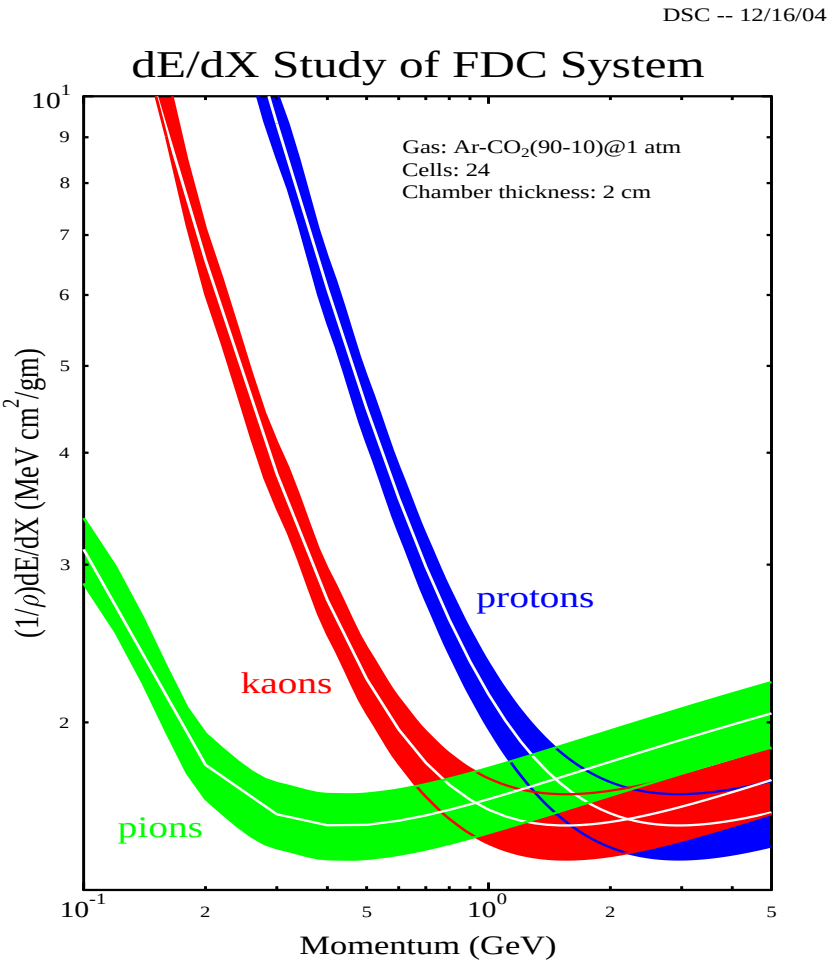

Figure 3: Computation of the stopping power (plotted here as $\rho^{-1}dE/dX$) vs. momentum. The shaded bands represent the measurement resolution computed from eq.(11).

Eq.(3) gives the average energy loss in a material layer of thickness x. However, there are fluctuations about this mean value, with a long tail toward higher energy loss (this is a Landau distribution). The most probable energy loss can be parameterized as [2]:

$$E_{prob} = \frac{t}{\beta^2}\left[\ln\left(\frac{2m_e c^2\gamma^2 t}{I}\right) - \beta^2 + 0.432\right], \tag{4}$$

where t is proportional to the layer thickness x and is defined in a gas at pressure $\mathcal{P}$ by:

$$t(MeV) = 0.1536\frac{Z\rho}{A\mathcal{P}}x, \tag{5}$$

with x in units of gm/cm^2. For the calculations that follow in this document, however, the form of dE/dX from eq.(3) will be employed.

3.1 Mean Excitation Potential

The mean excitation potential I for the medium has been estimated from actual dE/dX measurements and a semi-empirical formula for I vs. Z fitted to the points. There are several parameterizations available in the literature. The form employed here is given by [1]:

$$\begin{aligned} \frac{I(eV)}{Z} &= 12 + \frac{7}{Z} \qquad Z < 13, \\ \frac{I(eV)}{Z} &= 9.76 + 58.8Z^{-1.19} \quad Z \geq 13. \end{aligned} \tag{6}$$

3.2 Density Correction

The relativistic rise saturates at higher energies due to the density correction term because the medium becomes polarized, effectively reducing the influence of distant electrons. The density correction has been parameterized and is given by [3],

$$\begin{aligned} \delta &= 0 && \text{for } X = \ln \beta\gamma < X_0, \\ \delta &= 4.605X + C_0 + a(X_1 - X)^m && \text{for } X_0 < X < X_1, \\ \delta &= 4.605X + C_0 && \text{for } X > X_1 \end{aligned} \tag{7}$$

The quantities X_0, X_1, C_0, a, and m depend on the absorbing material. However the parameters for all common gases are very similar. Using values of X_0=1.74, X_1=4.24, a=0.10, and m=3.4, which are the constants associated with air [1], along with the form of C_0 given by:

$$C_0 = -\left(2\ln\frac{1}{h\nu_p} + 1\right), \tag{8}$$

where $h\nu_p$ is the so-called plasma energy of the material, i.e.,

$$\nu_p = \sqrt{\frac{N_e e^2}{\pi m_e}}, \tag{9}$$

where $N_e = N_A \rho Z/A$ is the density of electrons, gives a result of $\delta = 0$ for the energy range associated with GlueX.

3.3 Shell Correction

The form of the shell correction can be determined empirically based on the form given in Ref. [1] which is valid for $\eta \geq 0.1$,

$$\begin{aligned} C(I,\eta) &= (0.422377\eta^{-2} + 0.0304043\eta^{-4} - 0.00038106\eta^{-6}) \times 10^{-6} I^2 \\ &\quad + (3.850190\eta^{-2} - 0.1667989\eta^{-4} + 0.00157955\eta^{-6}) \times 10^{-9} I^3, \end{aligned} \tag{10}$$

where $\eta = \beta\gamma$ and I is the mean excitation potential in unit of eV. For the range of momenta relevant in GlueX, down to 100 MeV/c or so, this correction term remains negligible.

3.4 Mixtures

The Bethe-Bloch formula as written above is really for pure elements. However it is still applicable for mixtures such as Ar-CO_2 and Ar-CH_4 with some minor modifications. These changes are to replace Z, A, ρ, C, and I with the appropriate values for the mixture under consideration.

4 FDC Studies

In the computations carried out in this document, the sensitivity to two different gas mixtures has been considered. These gas mixtures are Argon (90%) - CO_2 (10%) and Argon (50%) - CH_4 (50%). These are two representative and typical gas mixtures for drift chamber systems. They can be used to show typical values for energy loss and resolution.

The dE/dX resolution of a drift chamber system (or a gas-sampling device in general) has been determined empirically to obey the relation [4, 5]:

$$\sigma_{dE/dX} = 0.41 n^{-0.43} (x\mathcal{P})^{-\prime.\ni\in}, \tag{11}$$

where n is the number of dE/dX measurements made (which here is given by the number of anode layers in the FDC system – 24), x is the sampling thickness (or the thickness of a single FDC chamber layer – 2 cm), and $\mathcal{P}$ is the pressure of the system (here the FDC is assumed to operate at $\mathcal{P}$=1 atm). While this expression is used in the current work to estimate the dE/dX resolution, a better fit can be obtained by replacing $(x\mathcal{P})$ in eq.(11) with $6.83 N_e x(cm)\mathcal{P}(\dashv\sqcup\Updownarrow)/\mathcal{I}(\rceil\mathcal{V})$, where N_e is the number of electrons per molecule [6].

Given the modified Bethe-Bloch expression in eq.(3) and the form of the dE/dX resolution in eq.(11), one can predict the separation of two particles of mass M_1 and M_2 in terms of the number of sigmas via:

$$\mathcal{R} = \frac{dE/dX(M_1) - dE/dX(M_2)}{\sigma_{dE/dX}}. \tag{12}$$

Of interest for the current design of the FDC system is the region in momentum over which pions and kaons, as well as kaons and protons, can be separated. A typical guesstimate is that separation of the different hadron species can be achieved as long as $\mathcal{R} > 2\sigma$. This assumption is used here as our guide.

The main results of this study are shown in Fig. 4 which plots $\mathcal{R}$ vs. momentum P highlighting where K/π and K/p separation is possible within the current FDC system. For these calculations only the chamber gas medium is considered. The mixtures considered here are Argon/CO_2 (90%-10%) and Argon/CH_4 (50%-50%) at 1 atm. Note that resolution considering 24 FDC layers of 2 cm thickness is 8.37%. If we consider an FDC system consisting only of 3 6-layer packages, this resolution worsens to 9.48%.

Measured resolutions in several different detector systems are highlighted in Table 2 [4]. These different detector packages rely in one way or another on using their gas-filled chambers for dE/dX measurements and particle identification.

Detector	n	$x(cm)$	P	Expected resol.	Measured resol.
Aleph	344	0.36	1 atm	4.6%	4.5%
TPC/PEP	180	0.5	8.5 atm	2.8%	2.5%
OPAL	159	0.5	4 atm	3.0%	3.1%
MKII/SLC	72	0.833	1 atm	6.9%	7.0%

Table 2: Measured resolutions are compared to the expected dE/dX resolutions from eq.(11).

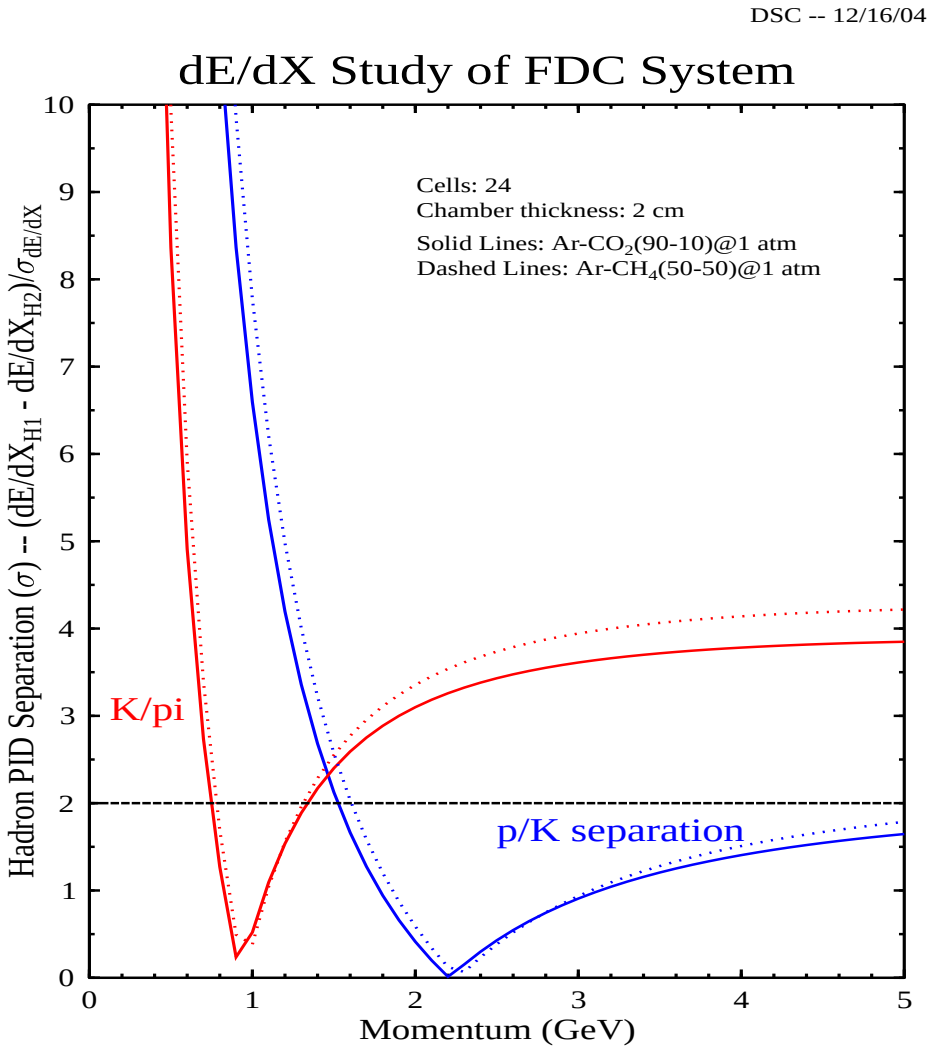

Figure 4: Calculation of the separation (in σ) from eq.(12) between different particle species vs. momentum. The calculations are shown for two different gas mixtures with the current FDC system geometry design assuming all 24 layers are used in the measurement.

The main results of Fig. 4 indicate that with the current FDC system design K/π separation is possible below 0.8 GeV/c and above 1.5 GeV/c. As well, K/p separation can be achieved below 1.7 GeV/c.

This assumes that all 24 measurement layers in the FDC can be employed. This might be a reasonable expectation if the electrostatics are such that the fields can be considered as uniform throughout the FDC system. However in reality some fraction of the chamber hit pulses are removed from the computation to reduce the high side tail due to Landau fluctuations (up to 40-50% of the hits in some cases) and some fraction of the low pulse heights are removed to reduce noise effects (roughly 5-10% of the hits). Thus the results in Fig. 4 with n=24 are a highly optimistic scenario.

In reality we should consider dE/dX resolution for the GlueX FDC to be closer to 11.3% using eq.(11) as a parameterization of the dE/dX resolution with n=12. The resolution for this condition is shown in Fig. 5. This would modify the ranges given above associated with Fig. 4 and indicates that K/π separation is possible below 0.7 GeV/c and above 1.7 GeV/c. As well, K/p separation can be achieved below 1.3 GeV/c.

If each sampling is independent, which should certainly be the case in the FDC measurement scheme, and there are no other sources of error (such as electrical noise), then the resolution will scale as $n^{-0.5}$. Since the power on n in eq.(11) is larger than that on x, for a fixed total length one obtains a better resolution for finer sampling. However, at some point the number of primary ionizations along the incident charged particle path limits the scale on x. Typically, the critical sampling size is about a few mm [4].

5 Particle Identification Approach

The information from this section has been distilled from the thesis by Andrei Gritsan [7] who discusses particle identification via dE/dX from the CLEO experiment at Cornell's CESR facility. This section is designed to introduce how the accumulated information is actually used to determine the particle type.

Particle identification using dE/dX begins by summing all of the pulse heights associated with the full set of hits for a given track into a single parameter (Σ_{ph}). As alluded to in Section 4, some fraction of the high pulse height hits are typically removed to reduce the high-side tail due to Landau fluctuations and some small fraction of the low pulse height hits are removed to reduce noise effects. Also the individual track hit pulse heights are corrected for drift distance and entrance angle broadening. If one hit is a candidate for more than one track, it is not used in the dE/dX measurement.

Particle identification then proceeds by comparing the measured pulse height to that expected for a given particle type using:

$$\Delta_{xx} = \frac{\Sigma_{ph} - MEAN_{xx}}{\sigma_{xx}}, \tag{13}$$

where here xx= e, μ, π, K, or p, and $MEAN_{xx}$ and σ_{xx} represent the mean and sigma of the ionization loss dE/dX measurements. These parameters in general depend upon the charged track parameters, and are typically parameterized in terms of the track momentum and angle for each particle species. Note that the parameter Δ_{xx} is designed to have a Gaussian

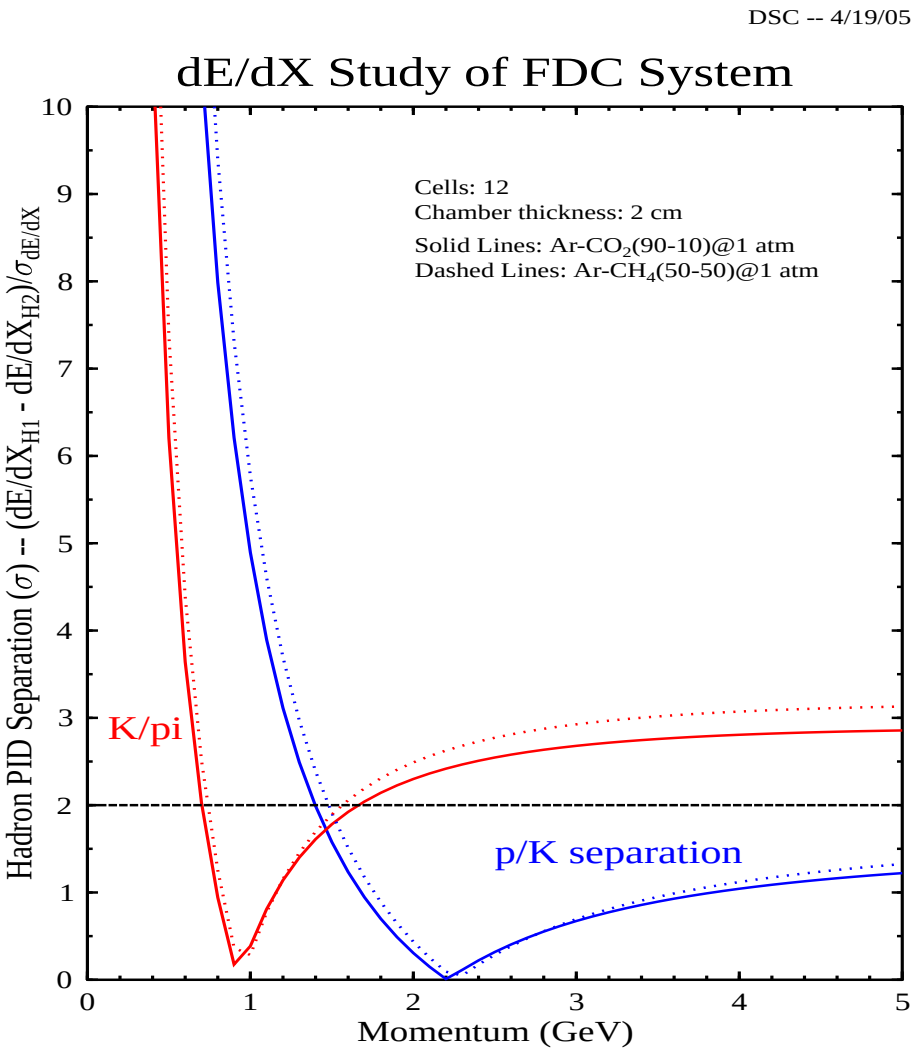

Figure 5: Calculation of the separation (in σ) from eq.(12) between different particle species vs. momentum. The calculations are shown for two different gas mixtures with the current FDC system geometry design assuming only 12 layers are used in the measurement.

distribution centered at zero with a width of unity for the correct particle identification hypothesis. The particle type hypothesis that best matches Δ_{xx}=0 is the assigned particle type.

The resolution of Σ_{ph} depends on the single hit resolution and the number of chamber hits used in the dE/dX measurement. The findings from CLEO indicate:

$$\sigma_{\Sigma_{ph}} = \frac{\sigma_{single\ hit}}{(N_{hits})^{0.428}}. \tag{14}$$

References

[1] W.R. Leo, "Techniques for Nuclear and Particle Physics Experiments", Second Revised Edition, Springer-Verlag, 24 (1994).

[2] R. Talman, "On the Statistics of Particle Identification Using Ionization", Nucl. Inst. and Meth. **159**, 189 (1979).

[3] R.M. Sternheimer *et al.*, Atomic Data and Nuclear Data Tables, **30**, 261 (1984).

[4] H. Yamamoto, "dE/dX Particle Identification For Collider Detectors", hep-ex/9912024, (1999).

[5] A.H. Walenta *et al.*, Nucl. Inst. and Meth. **161**, 45 (1979).

[6] W.W.M. Allison and J.H. Cobb, Ann. Rev. Pert. Sci **30**, 253 (1980).

[7] A. Gritsan, Ph.D. thesis, University of Colorado (unpublished), (2000).